

# Spatial properties of entangled photon pairs generated in nonlinear layered structures

Jan Peřina, Jr.

*Palacký University, RCPTM, Joint Laboratory of Optics,  
17. listopadu 12, 771 46 Olomouc, Czech Republic\**

A spatial quantum model of spontaneous parametric down-conversion in nonlinear layered structures is developed expanding the interacting vectorial fields into monochromatic plane waves. A two-photon spectral amplitude depending on the signal- and idler-field frequencies and propagation directions is used to derive transverse profiles of the emitted fields as well as their spatial correlations. Intensity spatial profiles and their spatial correlations are mainly determined by the positions of transmission peaks formed in these structures with photonic bands. A method for geometry optimization of the structures with respect to efficiency of the nonlinear process is suggested. Several structures composed of GaN/AlN layers are analyzed as typical examples. They allow the generation of photon pairs correlated in several emission directions. Photon-pair generation rates increasing better than the second power of the number of layers can be reached. Also structures efficiently generated photon pairs showing anti-bunching and anti-coalescence can be obtained. Three reasons for splitting the correlated area in photonic-band-gap structures are revealed: zig-zag movement of photons inside the structure, spatial symmetry and polarization-dependent properties. Also spectral splitting can be observed in these structures.

PACS numbers: 42.65.Lm, 42.70.Qs, 42.50.Dv

## I. INTRODUCTION

The first temporal correlations between the signal and idler photons generated in the process of spontaneous parametric down-conversion (SPDC) were observed already more than thirty years ago [1]. They manifested quantum entanglement in the common state of both photons generated in one quantum event of the spontaneous nonlinear process [2]. Since then the understanding of properties of such photon pairs has grown enormously. Polarization properties and namely polarization entanglement between the signal and idler photons originating in tensorial character of the nonlinear susceptibility have attracted the greatest attention from the very beginning. The reason lies in the simplicity of such states described in the Hilbert space with dimension  $2 \times 2$ . This made these states easily experimentally accessible. Despite their simplicity, such states have allowed to reveal many substantial features of quantum physics related to correlations between subsystems [3]. Violation of the Bell inequalities that ruled out neoclassical theories [4], the effect of collapse of a wave-function [4] and the ability of teleportation of a quantum state [5] belong to the most important.

In the time domain, both photons occur in a very narrow temporal window [1] because they are emitted at one instant after the annihilation of a pump photon. Moreover the conservation law of energy dictates entanglement among monochromatic components of the signal and idler fields [2]. This entanglement leads to a typical finite entanglement time between the detection instants of the signal and idler photons observable in a Hong-Ou-

Mandel interferometer [1] or sum-frequency generation of the paired photons [6, 7]. These properties have been extensively studied namely in connection with the generation by pulsed pump fields [8, 9] that allows precise synchronization of photons from different photon pairs.

Spatial properties of photon pairs have attracted attention last. Correlations in the transverse planes of the signal and idler photons occur here due to geometric properties of a photon-pair source and pump-beam spatial profile. They originate in the necessity of reaching good spatial phase matching of the interacting fields [2] that results in an efficient nonlinear process. For example, the sum of wave vectors of the signal and idler fields has to approximately give the wave vector of the pump field to observe an efficient photon-pair generation in an extended bulk crystal using collimated pumping. This results in strong correlations in emission directions of the signal and idler photons [10–12]. These correlations may even be exploited to 'transfer' spatial properties of the pump beam into spatial correlations of the signal and idler beams [13, 14]. We may observe analogy between spatial and spectral correlations (entanglement) of two photons in a pair. Similarly as spectral correlations may be tailored by a pump-field spectral profile, spatial correlations may be controlled by a pump-beam spatial profile. Also signal and idler electric-field phase variations in the transverse plane belong to important characteristics of photon pairs. They can be quantified in terms of eigenstates of the angular orbital momentum operator [15]. Under certain conditions, entanglement between such states in the signal and idler fields has been observed [16, 17]. Experimentally, spatial correlations can be conveniently measured by moving a fiber tip in the transverse plane, as it has been done, e.g., in [18]. The use of an intensified CCD camera has provided a more elegant way for the experimental investigations of spatial

---

\*Electronic address: perinaj@prfnw.upol.cz

correlations [19, 20]. Spatial correlations between the down-converted beams have also been extensively used for quantum ghost imaging [21]. We note that spatial correlations occur not only in spontaneous regime, they have been found also in the regime with prevailing stimulated emission [22, 23].

All these forms of entanglement are potentially interesting both for fundamental physical experiments and practical applications including metrology [24], quantum cryptography [25] and quantum-information processing [3]. In principle, all these forms of entanglement can occur simultaneously depending on the source of photon pairs. However, usual sources of photon pairs are constructed such that only one or two forms of entanglement (e.g., polarization and spectral) are found and may efficiently be experimentally exploited.

The effort to generate entangled photon pairs extended over as many basis states as possible (and defined in several degrees of freedom) and to modify 'the structure of entanglement' belong together with the effort to enhance quantum efficiency of the generation process to the leit-motifs of the development in this field. Bulk nonlinear crystals that were nearly exclusively used at the beginning have been gradually replaced by more complex and efficient nonlinear structures including poled nonlinear materials [6, 26–28], nonlinear waveguides [29–31] and nonlinear photonic structures [32]. Nonlinear photonic structures are extraordinarily interesting because they allow efficient photon-pair generation owing to enhanced electric-field amplitudes observed inside structures with photonic band-gaps [33, 34] on one side, they also allow relatively wide tailoring of properties of the emitted photon pairs on the other side [35–37]. Structured nonlinear fibers that rely on four-wave mixing [38–40] represent a typical example. Or waveguides with Bragg mirrors [41, 42] can be mentioned as perspective sources.

In the article, we consider systems composed of parallel nonlinear layers. Back-scattering of the fields on the boundaries between layers provides suitable conditions for the enhancement of electric-field amplitudes under certain conditions [43]. Moreover, spatial properties of photon pairs can be efficiently tailored using parameters of these systems (e.g., the number of layers). Nonlinear layered structures have already been studied in the simplified geometry both in the framework of classical [36] and quantum [37] descriptions. Here, we generalize the quantum model present in [37] to the real spatial geometry including vectorial character of the interacting fields. This allows us to study transverse intensity profiles of the down-converted beams as well as correlated areas of the signal and idler photons considering typical layered structures made of GaN/AlN. We note that GaN/AlN structures with random layers' lengths have already been studied as sources of photon pairs with ultra-narrow spectral widths that originated in an optical analog of Anderson localization of the down-converted fields [44, 45]. It has also been shown that GaN/AlN nonlinear layers allow the generation of photon-pair states antisymmetric with

respect to the exchange of the signal- and idler-field frequencies that exhibit anti-bunching and anti-coalescence [46].

The investigated layered structures as sources of photon pairs can be compared with other photon-pair sources with respect to intensity transverse profile, correlated area and efficiency of photon-pair generation as follows. The vast majority of photon-pair sources including wave-guiding structures and nonlinear crystals with/without poling are designed such that the signal (and similarly the idler) photon is generated into one compact and small emission area. In some sources, bulk crystals are cut in such a way that the spatial symmetry allows to generate photons around the whole cone surface [12]. In this case the generated state is entangled also in the wave vectors of the signal and idler photons. As the Hilbert space corresponding to this degree of freedom has a greater number of independent states we obtain a higher-dimensional entangled state. In case of layered structures, the signal (and idler) photon can even be generated around several concentric cone surfaces depending on complexity of the structure. This even enlarges the number of independent states in the transverse area making the generated state suitable for 'parallel processing' of quantum information in the transverse plane. As for correlated areas, they are described by compact profiles (usually of an elliptical shape) in all common photon-pair sources with cw pumping. Splitting of correlated areas into several well-separated parts is a distinguished property of nonlinear layered structures. Even three different mechanisms leading to this splitting exist in layered structures: zig-zag movement of photons inside the structure, spatial symmetry and polarization-dependent properties. The last two mechanisms may in principle occur also in other photon-pair sources. However, enhancement of the fields' amplitudes inside a structure is needed to make them significant. Finally, periodically-poled nonlinear crystals provide the greatest photon-pair fluxes. On the other hand, wave-guiding structures including nonlinear planar wave-guides and nonlinear structured fibers have the greatest nonlinear conversion efficiencies due to the transverse confinement of the interacting fields. However, they allow for only moderate pumping intensities because of a possible material damage and competing nonlinear processes. Nonlinear layered structures lie in the middle in this comparison. They provide greater nonlinear conversion efficiencies than bulk crystals owing to enhanced electric-field amplitudes along the propagation direction. Compared to wave-guiding structures, their nonlinear conversion efficiencies are lower because the 'fields' confinement' is only in one dimension. On the other hand, similar pumping intensities as those used for bulk crystals can be applied.

The paper is organized as follows. A spatial vectorial quantum model of SPDC in layered media is present in Sec. II and provides quantities characterizing the emitted photon pairs. A systematic method for designing efficient nonlinear structures is described in Sec. III. Transverse

intensity profiles and correlated areas are discussed in Sec. IV using structures with different numbers of layers. Conclusions are drawn in Sec. V.

## II. SPATIAL QUANTUM MODEL OF SPONTANEOUS PARAMETRIC DOWN-CONVERSION

Nonlinear Hamiltonian  $\hat{H}_{\text{int}}$  characterizing SPDC in a nonlinear medium of volume  $\mathcal{V}$  at time  $t$  can be written in the form [2]:

$$\hat{H}_{\text{int}}(t) = \epsilon_0 \int_{\mathcal{V}} d\mathbf{r} \mathbf{d}(\mathbf{r}) : \left[ \mathbf{E}_p^{(+)}(\mathbf{r}, t) \hat{\mathbf{E}}_s^{(-)}(\mathbf{r}, t) \hat{\mathbf{E}}_i^{(-)}(\mathbf{r}, t) + \text{h.c.} \right]. \quad (1)$$

In Eq. (1),  $\mathbf{d}$  stands for a third-order tensor of nonlinear coefficients and the symbol  $:$  means shorthand of the tensor  $\mathbf{d}$  with respect to its three indices. A strong pump field is described by the positive-frequency part  $\mathbf{E}_p^{(+)}(\mathbf{r}, t)$  of its electric-field amplitude vector. A signal [idler] field at single-photon level is characterized by the negative-frequency part  $\hat{\mathbf{E}}_s^{(-)}(\mathbf{r}, t)$  [ $\hat{\mathbf{E}}_i^{(-)}(\mathbf{r}, t)$ ] of its electric-field operator amplitude. Symbol  $\epsilon_0$  denotes permittivity of vacuum whereas h.c. stands for the Hermitian conjugate term.

The positive-frequency amplitudes  $\mathbf{E}_m^{(+)}(\mathbf{r}, t)$  of the interacting fields ( $m = p, s, i$ ) can be in general decomposed into plane waves with wave vectors  $\mathbf{k}_m$  and amplitudes  $\mathbf{E}_m^{(+)}(\mathbf{k}_m)$ :

$$\mathbf{E}_m^{(+)}(\mathbf{r}, t) = \frac{1}{(\sqrt{2\pi})^3} \int d^3\mathbf{k}_m \mathbf{E}_m^{(+)}(\mathbf{k}_m) \exp(i\mathbf{k}_m \mathbf{r} - i\omega_m t); \quad (2)$$

$\omega_m$  is the frequency of field  $m$  determined in accordance with dispersion relations.

Considering the incident and un-depleted pump field, we assume that its temporal spectrum  $\mathcal{E}_p(\omega_p)$  as well as spatial spectrum  $\mathcal{E}_p^{\text{tr}}(k_{px}, k_{py})$  in the transverse plane are given. In this case, the decomposition of amplitude  $\mathbf{E}_p^{(+)}(\mathbf{r}, t)$  in Eq. (2) can be rewritten as:

$$\begin{aligned} \mathbf{E}_p^{(+)}(\mathbf{r}, t) &= \frac{1}{(\sqrt{2\pi}c)^3} \int_{-\pi/2}^{\pi/2} \sin(\vartheta_p) d\vartheta_p \int_{-\pi/2}^{\pi/2} d\psi_p \\ &\int_0^\infty \omega_p^2 d\omega_p \mathcal{E}_p(\omega_p) \mathcal{E}_p^{\text{tr}}[k_{p,x}(\boldsymbol{\Omega}_p), k_{p,y}(\boldsymbol{\Omega}_p)] \\ &\times \exp[ik_{p,x}(\boldsymbol{\Omega}_p)x + ik_{p,y}(\boldsymbol{\Omega}_p)y] \sum_{\alpha=\text{TE, TM}} \mathbf{E}_{p,\alpha}^{(+)}(z, \boldsymbol{\Omega}_p) \\ &\times \exp(-i\omega_p t); \end{aligned} \quad (3)$$

using the vector  $\boldsymbol{\Omega}_p \equiv (\omega_p, \vartheta_p, \psi_p)$  of 'spherical coordinates'  $\omega_p$ ,  $\vartheta_p$  and  $\psi_p$ . Speed of light in vacuum is denoted as  $c$ . Assuming for simplicity air around the structure the  $x$  and  $y$  components of wave vector  $\mathbf{k}_p$  in front of the

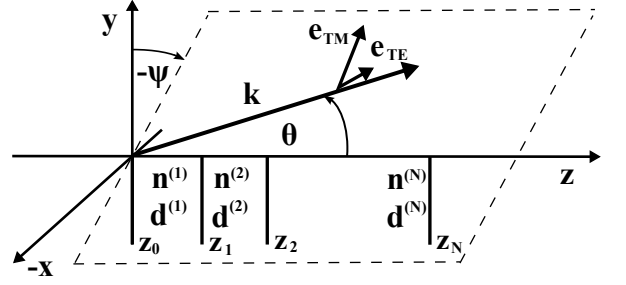


FIG. 1: Scheme of the structure and used coordinate system. A plane wave with wave vector  $\mathbf{k}$  propagates along the radial emission angle  $\vartheta$  and azimuthal emission angle  $\psi$ . The radial emission angle  $\vartheta$  is measured in the plane of incidence from the  $+z$  axis. The azimuthal emission angle  $\psi$  gives rotation in the  $xy$  plane beginning from the  $+y$  axis and rotating towards the  $-x$  axis. Vectors  $\mathbf{e}_{\text{TE}}$  and  $\mathbf{e}_{\text{TM}}$  give polarization directions of TE and TM waves determined with respect to the plane of incidence. Symbols  $z_i$  for  $i = 0, \dots, N$  identify  $z$  positions of the boundaries being perpendicular to the  $z$  axis;  $n^{(l)}$  [ $\mathbf{d}^{(l)}$ ] means index of refraction [tensor of nonlinear coefficients] in an  $l$ th layer.

structure are given as:

$$\begin{aligned} k_{p,x}(\boldsymbol{\Omega}_p) &= -\frac{\omega_p \sin(\psi_p) \sin(\vartheta_p)}{c}, \\ k_{p,y}(\boldsymbol{\Omega}_p) &= \frac{\omega_p \cos(\psi_p) \sin(\vartheta_p)}{c}. \end{aligned} \quad (4)$$

The decomposition of pump-field amplitude  $\mathbf{E}_p^{(+)}$  into TE and TM waves as given in Eq. (3) is done with respect to the plane of incidence of the wave with wave vector  $\mathbf{k}_p$  propagating through the layered structure (see Fig. 1 for a scheme of the structure). We note that projections of  $\mathbf{k}$  vectors into the planes of boundaries are conserved through the structure. The pump-field amplitudes  $\mathbf{E}_{p,\alpha}^{(+)}$  introduced in Eq. (3) describe field evolution along the  $z$  axis where the field undergoes back-scattering at the boundaries.

Considering a structure with  $N$  layers and boundaries perpendicular to the  $z$  axis localized at positions  $z_n$ ,  $n = 0, \dots, N$ , the pump-field amplitude  $\mathbf{E}_{p,\alpha}^{(+)}$  can be written in the form (for more details, see [37]):

$$\begin{aligned} \mathbf{E}_{p,\alpha}^{(+)}(z, \boldsymbol{\Omega}_p) &= \text{rect}_{-\infty, z_0}(z) \sum_{a=F,B} A_{p_a,\alpha}^{(0)}(\boldsymbol{\Omega}_p) \\ &\times \mathbf{e}_{p_a,\alpha}^{(0)}(\boldsymbol{\Omega}_p) \exp\left[iK_{p_a,z}^{(0)}(\boldsymbol{\Omega}_p)(z - z_0)\right] \\ &+ \sum_{l=1}^N \text{rect}_{z_{l-1}, z_l}(z) \sum_{a=F,B} A_{p_a,\alpha}^{(l)}(\boldsymbol{\Omega}_p) \\ &\times \mathbf{e}_{p_a,\alpha}^{(l)}(\boldsymbol{\Omega}_p) \exp\left[iK_{p_a,z}^{(l)}(\boldsymbol{\Omega}_p)(z - z_{l-1})\right] \\ &+ \text{rect}_{z_N, \infty}(z) \sum_{a=F,B} A_{p_a,\alpha}^{(N+1)}(\boldsymbol{\Omega}_p) \\ &\times \mathbf{e}_{p_a,\alpha}^{(N+1)}(\boldsymbol{\Omega}_p) \exp\left[iK_{p_a,z}^{(N+1)}(\boldsymbol{\Omega}_p)(z - z_N)\right]; \end{aligned}$$

$$\alpha = \text{TE, TM.} \quad (5)$$

The function  $\text{rect}_{z_a, z_b}(z)$  equals one for  $z_a \leq z \leq z_b$  and is zero otherwise. Symbols  $\mathbf{e}_{p_F, \alpha}^{(l)}$  and  $\mathbf{e}_{p_B, \alpha}^{(l)}$  denote polarization vectors of  $\alpha$  waves for forward- and backward-propagating fields with respect to the  $+z$  axis, respectively.

The  $z$  component  $K_{p_a, z}^{(l)}(\boldsymbol{\Omega}_p)$  of wave vector in an  $l$ th layer belonging to wave  $a$  with frequency  $\omega_p$  and propagating in direction  $(\vartheta_p, \psi_p)$  in front of the structure can be expressed as:

$$K_{p_a, z}^{(l)}(\boldsymbol{\Omega}_p) = \pm \frac{n_p^{(l)}(\omega_p)\omega_p}{c} \cos(\vartheta_p^{(l)}), \quad (6)$$

where the sign  $+$  ( $-$ ) is appropriate for a forward- (backward-) propagating wave. Index of refraction of the pump field in an  $l$ th layer is denoted as  $n_p^{(l)}$ . As we assume that the layered structure is surrounded by air, we have  $n_p^{(0)} = n_p^{(N+1)} = 1$ . The propagation angle  $\vartheta_p^{(l)}$  in the  $l$ th layer is then derived from Snell's law:

$$n_p^{(0)} \sin(\vartheta_p^{(0)}) = n_p^{(l)} \sin(\vartheta_p^{(l)}), \quad l = 1, \dots, N+1; \quad (7)$$

$$\vartheta_p^{(0)} \equiv \vartheta_p.$$

The coefficients  $A_{p_F, \alpha}^{(l)}(\boldsymbol{\Omega}_p)$  and  $A_{p_B, \alpha}^{(l)}(\boldsymbol{\Omega}_p)$  introduced in Eq. (5) determine amplitudes of  $\alpha$  waves with frequency  $\omega_p$  propagating forward and backward, respectively, in the  $(\vartheta_p, \psi_p)$  direction. These coefficients are derived from Fresnel's relations at the boundaries using, e.g., the transfer-matrix formalism [43]. Values of the coefficients  $A_{p_F, \alpha}^{(0)}(\boldsymbol{\Omega}_p)$  and  $A_{p_B, \alpha}^{(N+1)}(\boldsymbol{\Omega}_p)$  for  $\alpha = \text{TE, TM}$  characterize the pump fields incident on the structure from both sides and represent the boundary conditions. The transfer-matrix formalism has been elaborated in detail in [37] for layered structures. The coefficients  $A^{(l)}$  of the fields with wave vectors lying in the plane of incidence given by an angle  $\psi_p$  are given by Eq. (23) of Ref. [37].

The signal and idler fields are at single-photon level in the spontaneous process and so they have to be treated using quantum theory [2]. Their electric-field operator amplitudes in the layered structure can be decomposed into plane waves using Eq. (1) and subsequently described in analogy to the pump field. Using the 'spherical coordinates'  $\omega_m, \vartheta_m$  and  $\psi_m$  and defining  $\boldsymbol{\Omega}_m = (\omega_m, \vartheta_m, \psi_m)$ ,  $m = s, i$ , we can express the positive-frequency part  $\hat{\mathbf{E}}_m^{(+)}$  of the electric-field operator amplitude of mode  $m$  as:

$$\begin{aligned} \hat{\mathbf{E}}_m^{(+)}(\mathbf{r}, t) &= \frac{1}{c^3} \int_{-\pi/2}^{\pi/2} \sin(\vartheta_m) d\vartheta_m \int_{-\pi/2}^{\pi/2} d\psi_m \\ &\int_0^\infty \omega_m^2 d\omega_m \exp[ik_{m,x}(\boldsymbol{\Omega}_m)x + ik_{m,y}(\boldsymbol{\Omega}_m)y] \\ &\times \sum_{\alpha=\text{TE, TM}} \sqrt{\frac{\hbar\omega_m}{16\pi^3\epsilon_0}} \hat{\mathbf{a}}_{m,\alpha}(z, \boldsymbol{\Omega}_m) \exp(-i\omega_m t); \quad (8) \end{aligned}$$

$\hbar$  stands for the reduced Planck constant and  $\hat{\mathbf{E}}_m^{(-)} = \hat{\mathbf{E}}_m^{(+)\dagger}$ . The expression  $\sqrt{\hbar\omega_m/(16\pi^3\epsilon_0)}$  gives an electric-field amplitude per one photon with energy  $\hbar\omega_m$  propagating at speed  $c$ . The  $x$  and  $y$  components of wave vectors  $\mathbf{k}_m$  of the signal and idler fields ( $m = s, i$ ) are defined outside the structure:

$$\begin{aligned} k_{m,x}(\boldsymbol{\Omega}_m) &= -\frac{\omega_m \sin(\psi_m) \sin(\vartheta_m)}{c}, \\ k_{m,y}(\boldsymbol{\Omega}_m) &= \frac{\omega_m \cos(\psi_m) \sin(\vartheta_m)}{c}. \quad (9) \end{aligned}$$

The operator amplitudes  $\hat{\mathbf{a}}_{m,\alpha}(z, \boldsymbol{\Omega}_m)$  introduced in Eq. (8) can be derived in the considered layered structure in the form:

$$\begin{aligned} \hat{\mathbf{a}}_{m,\alpha}(z, \boldsymbol{\Omega}_m) &= \text{rect}_{-\infty, z_0}(z) \sum_{a=F, B} \hat{\mathbf{a}}_{m_a, \alpha}^{(0)}(\boldsymbol{\Omega}_m) \\ &\times \mathbf{e}_{m_a, \alpha}^{(0)}(\boldsymbol{\Omega}_m) \exp\left[iK_{m_a, z}^{(0)}(\boldsymbol{\Omega}_m)(z - z_0)\right] \\ &+ \sum_{l=1}^N \text{rect}_{z_{l-1}, z_l}(z) \sum_{a=F, B} \hat{\mathbf{a}}_{m_a, \alpha}^{(l)}(\boldsymbol{\Omega}_m) \\ &\times \mathbf{e}_{m_a, \alpha}^{(l)} \exp\left[iK_{m_a, z}^{(l)}(\boldsymbol{\Omega}_m)(z - z_{l-1})\right] \\ &+ \text{rect}_{z_N, \infty}(z) \sum_{a=F, B} \hat{\mathbf{a}}_{m_a, \alpha}^{(N+1)}(\boldsymbol{\Omega}_m) \\ &\times \mathbf{e}_{m_a, \alpha}^{(N+1)}(\boldsymbol{\Omega}_m) \exp\left[iK_{m_a, z}^{(N+1)}(\boldsymbol{\Omega}_m)(z - z_N)\right]; \\ &m = s, i; \quad \alpha = \text{TE, TM.} \quad (10) \end{aligned}$$

Here, the symbols  $\mathbf{e}_{m_F, \alpha}^{(l)}$  and  $\mathbf{e}_{m_B, \alpha}^{(l)}$  stand for polarization vectors of  $\alpha$  wave of field  $m$  propagating forward and backward, respectively. The annihilation operators  $\hat{\mathbf{a}}_{m_a, \alpha}^{(l)}(\boldsymbol{\Omega}_m)$  are defined at the end of an  $l$ th layer for the  $\alpha$  wave with frequency  $\omega_m$  of field  $m$  propagating along the direction  $(\vartheta_m, \psi_m)$  either forward ( $a = F$ ) or backward ( $a = B$ ).

The  $z$  component  $K_{m_a, z}^{(l)}(\boldsymbol{\Omega}_m)$  of wave vector in the  $l$ th layer is determined as:

$$\begin{aligned} K_{m_a, z}^{(l)}(\boldsymbol{\Omega}_m) &= \pm \frac{n_m^{(l)}(\omega_m)\omega_m}{c} \cos(\vartheta_m^{(l)}), \\ &m = s, i; \quad a = F, B. \quad (11) \end{aligned}$$

The sign  $+$  ( $-$ ) stands for a forward- (backward-) propagating wave and  $n_m^{(l)}$  gives index of refraction of field  $m$  in the  $l$ th layer. Snell's law provides the propagation angles  $\vartheta_m^{(l)}$  needed in the  $l$ th layer:

$$\begin{aligned} n_m^{(l)}(\omega_m) \sin(\vartheta_m^{(l)}) &= n_m^{(N+1)}(\omega_m) \sin(\vartheta_m^{(N+1)}), \\ &l = 0, \dots, N; \quad (12) \end{aligned}$$

$$\vartheta_m^{(N+1)} \equiv \vartheta_m.$$

The operators  $\hat{\mathbf{a}}_{m_a, \alpha}^{(l)}(\boldsymbol{\Omega}_m)$  for  $l = 0, \dots, N+1$  and fixed  $m, \alpha, \omega_m, \vartheta_m$ , and  $\psi_m$  are connected by unitary transformations at boundaries (Fresnel's relations) and

free-field propagation transformations. This means that the usual boson commutation relations obeyed by the incident fields are 'transferred' through the structure and the only nonzero commutation relations [47] are the following ones:

$$[\hat{a}_{m_a,\alpha}^{(l)}(\mathbf{\Omega}_m), \hat{a}_{m'_a,\alpha'}^{(l')\dagger}(\mathbf{\Omega}'_{m'})] = \frac{c^2}{|\sin(\vartheta_m)|\omega_m^2} \delta_{m,m'} \delta_{a,a'} \delta_{\alpha,\alpha'} \delta_{l,l'} \delta(\omega_m - \omega'_{m'}) \delta(\vartheta_m - \vartheta'_{m'}) \delta(\psi_m - \psi'_{m'}). \quad (13)$$

The transfer-matrix formalism allows to express the operators  $\hat{a}_{m_a,\alpha}^{(l)}(\mathbf{\Omega}_m)$  in terms of the operators  $\hat{a}_{m_F,\alpha}^{(N+1)}(\mathbf{\Omega}_m)$  and  $\hat{a}_{m_B,\alpha}^{(0)}(\mathbf{\Omega}_m)$  describing the outgoing fields. The appropriate relations valid for fields with wave vectors lying in the plane of incidence given by an angle  $\psi_m$  are given in Eq. (21) of Ref. [37].

The generation of a photon pair in the process of SPDC governed by the Hamiltonian  $\hat{H}_{\text{int}}$  in Eq. (1) is described by a perturbation solution of the Schrödinger equation to the first order at time  $t \rightarrow \infty$  assuming an incident vacuum state  $|\text{vac}\rangle$  in the signal and idler fields at time  $t \rightarrow -\infty$ . The resulting state  $|\psi\rangle_{s,i}^{\text{out}}$  can be derived in the form:

$$\begin{aligned} |\psi\rangle_{s,i}^{\text{out}} &= |\text{vac}\rangle - \frac{i}{2c^8} \sum_{l=1}^N \sum_{a,b,g=F,B} \sum_{\alpha,\beta,\gamma=\text{TE,TM}} \prod_{m=p,s,i} \int_{-\pi/2}^{\pi/2} \sin(\vartheta_m) d\vartheta_m \int_{-\pi/2}^{\pi/2} d\psi_m \int_0^\infty \omega_m^2 d\omega_m \\ &\quad \sqrt{\omega_s \omega_i} \mathcal{E}_p(\omega_p) \mathcal{E}_p^{\text{tr}}(k_{p,x}, k_{p,y}) \delta(\omega_p - \omega_s - \omega_i) \\ &\quad \times \delta[k_{p,x} - k_{s,x} - k_{i,x}] \delta[k_{p,y} - k_{s,y} - k_{i,y}] \\ &\quad \times \mathbf{d}^{(l)} : \mathbf{e}_{p_a,\alpha}^{(l)}(\mathbf{\Omega}_m) \mathbf{e}_{s_b,\beta}^{(l)*}(\mathbf{\Omega}_s) \mathbf{e}_{i_g,\gamma}^{(l)*}(\mathbf{\Omega}_i) \\ &\quad \times \exp\left[\frac{i}{2} \Delta K_{p_a s_b i_g, z}^{(l)}(\mathbf{\Omega}_p, \mathbf{\Omega}_s, \mathbf{\Omega}_i) L_l\right] \\ &\quad \times L_l \text{sinc}\left[\frac{1}{2} \Delta K_{p_a s_b i_g, z}^{(l)}(\mathbf{\Omega}_p, \mathbf{\Omega}_s, \mathbf{\Omega}_i) L_l\right] \\ &\quad \times A_{p_a,\alpha}^{(l)}(\mathbf{\Omega}_m) \hat{a}_{s_b,\beta}^{(l)\dagger}(\mathbf{\Omega}_s) \hat{a}_{i_g,\gamma}^{(l)\dagger}(\mathbf{\Omega}_i) |\text{vac}\rangle. \end{aligned} \quad (14)$$

The functions  $\Delta K_{p_a s_b i_g, z}^{(l)}(\mathbf{\Omega}_p, \mathbf{\Omega}_s, \mathbf{\Omega}_i) = K_{p_a, z}^{(l)}(\mathbf{\Omega}_p) - K_{s_b, z}^{(l)}(\mathbf{\Omega}_s) - K_{i_g, z}^{(l)}(\mathbf{\Omega}_i)$  stand for phase mismatches in the  $l$ th layer. Symbol  $L_l$  means the length of  $l$ th layer ( $L_l = z_l - z_{l-1}$ ). The transverse wave vectors  $k_{m,x}(\mathbf{\Omega}_m)$  and  $k_{m,y}(\mathbf{\Omega}_m)$  for  $m = p, s, i$  are defined in Eqs. (4) and (9) and characterize the fields outside the structure. We note that the approach based on the solution of Schrödinger equation does not take into account surface SPDC that generates additional photon pairs [48, 49].

The phase-matching conditions in the transverse plane  $xy$  are described by two  $\delta$  functions in Eq. (14), that determine the emission direction  $(\vartheta_i, \psi_i)$  of an idler photon provided that the signal-photon emission direction  $(\vartheta_s, \psi_s)$  is given and the pump-field is in the form of a plane wave propagating in direction  $(\vartheta_p, \psi_p)$ . Simple ge-

ometric considerations provide the following formulas:

$$\begin{aligned} \psi_i &= \psi_p + \arctan\left[\frac{\omega_s \sin(\vartheta_s) \sin(\psi_p - \psi_s)}{\omega_p \sin(\vartheta_p) - \omega_s \sin(\vartheta_s) \cos(\psi_p - \psi_s)}\right], \\ \vartheta_i &= \arcsin\left[\frac{\omega_p \sin(\vartheta_p)}{\omega_i \cos(\psi_p - \psi_i)} - \frac{\omega_s \cos(\psi_p - \psi_s)}{\omega_i \cos(\psi_p - \psi_i)} \sin(\vartheta_s)\right]. \end{aligned} \quad (15)$$

If the pump beam is focused, the strict phase-matching conditions in the transverse plane formulated in Eq. (15) are relaxed and we arrive at correlation areas with finite spreads.

The expression in Eq. (14) for the state  $|\psi\rangle_{s,i}^{\text{out}}$  can be rewritten into the form containing only the outgoing creation operators  $\hat{a}_{m_F,\beta}^{(N+1)\dagger}(\mathbf{\Omega}_m)$  and  $\hat{a}_{m_B,\beta}^{(0)\dagger}(\mathbf{\Omega}_m)$  for  $m = s, i$  and  $\beta = \text{TE, TM}$  using the formulas in Eqs. (21) and (23) of Ref. [37]. The outgoing operators can be finally transformed into the polarization basis of the detector using a suitable unitary transformation. We assume that the detection plane is perpendicular to the field propagation direction  $(\vartheta, \psi)$  and its  $s$ -polarization (denoted as  $\perp$ ) is parallel to the horizontal plane  $xz$ ;  $p$ -polarization (denoted as  $\parallel$ ) is defined by the orthogonality conditions. Assuming field  $m$  ( $m = s, i$ ) at frequency  $\omega_m$  and propagating along the angles  $\vartheta_m$  and  $\psi_m$  the needed  $\vartheta_m$ - and  $\psi_m$ -dependent unitary transformation can be written in the form:

$$\begin{aligned} \begin{bmatrix} \hat{a}_{m_F,\text{TE}}^{(N+1)}(\mathbf{\Omega}_m) \\ \hat{a}_{m_F,\text{TM}}^{(N+1)}(\mathbf{\Omega}_m) \end{bmatrix} &= \begin{bmatrix} \cos(\zeta_m) & \sin(\zeta_m) \\ -\sin(\zeta_m) & \cos(\zeta_m) \end{bmatrix} \begin{bmatrix} \hat{a}_{m_F,\perp}(\mathbf{\Omega}_m) \\ \hat{a}_{m_F,\parallel}(\mathbf{\Omega}_m) \end{bmatrix}, \\ \begin{bmatrix} \hat{a}_{m_B,\text{TE}}^{(0)}(\mathbf{\Omega}_m) \\ \hat{a}_{m_B,\text{TM}}^{(0)}(\mathbf{\Omega}_m) \end{bmatrix} &= \begin{bmatrix} \cos(\zeta_m) & \sin(\zeta_m) \\ -\sin(\zeta_m) & \cos(\zeta_m) \end{bmatrix} \begin{bmatrix} \hat{a}_{m_B,\perp}(\mathbf{\Omega}_m) \\ \hat{a}_{m_B,\parallel}(\mathbf{\Omega}_m) \end{bmatrix}, \\ \zeta_m(\vartheta_m, \psi_m) &= \arccos\left[\frac{\cos(\psi_m)}{\sqrt{1 + \sin^2(\psi_m) \tan^2(\vartheta_m)}}\right] \\ &\quad \times \text{sign}(\psi_m), \quad m = s, i. \end{aligned} \quad (16)$$

The function  $\text{sign}$  gives the sign of its argument. The newly introduced annihilation operators  $\hat{a}_{m_b,\alpha}(\mathbf{\Omega}_m)$ ,  $m = s, i$ ,  $b = F, B$ ,  $\alpha = \parallel, \perp$ , describe the signal and idler fields in the polarization bases connected with the detectors.

The terms of state  $|\psi\rangle_{s,i}^{\text{out}}$  in Eq. (14) describing the created photon pair can be decomposed into four groups according to the propagation directions of the signal and idler photons with respect to the  $+z$  axis ( $FF$ ,  $FB$ ,  $BF$ ,  $BB$ ). Inside these groups there occur four contributions that differ in signal- and idler-photon polarization directions ( $\parallel\parallel$ ,  $\parallel\perp$ ,  $\perp\parallel$ ,  $\perp\perp$ ). Each contribution can be

written in the form:

$$\begin{aligned}
|\psi\rangle_{s_a, i_b}^{\alpha, \beta}(\mathbf{r}, t) &= \prod_{m=s, i} \int_{-\pi/2}^{\pi/2} \sin(\vartheta_m) d\vartheta_m \int_{-\pi/2}^{\pi/2} d\psi_m \\
&\int_0^\infty d\omega_m \phi_{ab}^{\alpha, \beta}(\boldsymbol{\Omega}_s, \boldsymbol{\Omega}_i) \hat{a}_{s_a, \alpha}^\dagger(\boldsymbol{\Omega}_s) \hat{a}_{i_b, \beta}^\dagger(\boldsymbol{\Omega}_i) |\text{vac}\rangle \\
&\times \exp[-i(\mathbf{k}_{s_a}^{\text{out}} + \mathbf{k}_{i_b}^{\text{out}})\mathbf{r}] \exp[i(\omega_s + \omega_i)t]; \\
&a, b = F, B; \quad \alpha, \beta = \parallel, \perp. \quad (17)
\end{aligned}$$

The wave vectors  $\mathbf{k}_{s_a}^{\text{out}}$  and  $\mathbf{k}_{i_b}^{\text{out}}$  characterize free-field evolution of the emitted signal and idler fields, respectively, outside the structure. The functions  $\phi_{ab}^{\alpha, \beta}(\boldsymbol{\Omega}_s, \boldsymbol{\Omega}_i)$  introduced in Eq. (17) characterize completely properties of the generated photon pair. It gives the probability amplitude of having an  $\alpha$ -polarized signal photon at frequency  $\omega_s$  propagating along direction  $(\vartheta_s, \psi_s)$  together with its  $\beta$ -polarized idler photon at frequency  $\omega_i$  propagating along direction  $(\vartheta_i, \psi_i)$  at the output  $ab$  of the structure.

Intensity spatial and spectral properties of a photon pair [37] can be conveniently derived from a density  $n_{ab}^{\alpha, \beta}$  of the mean photon-pair numbers belonging to the state  $|\psi\rangle_{s_a, i_b}^{\alpha, \beta}$ . The density  $n_{ab}^{\alpha, \beta}$  is defined along the expression

$$n_{ab}^{\alpha, \beta}(\boldsymbol{\Omega}_s, \boldsymbol{\Omega}_i) = \alpha_{s_a, i_b}^{\alpha, \beta} \langle \psi | \hat{n}_{s_a, \alpha}(\boldsymbol{\Omega}_s) \hat{n}_{i_b, \beta}(\boldsymbol{\Omega}_i) | \psi \rangle_{s_a, i_b}^{\alpha, \beta}. \quad (18)$$

The photon-number density operator  $\hat{n}_{m_a, \alpha}(\boldsymbol{\Omega}_m)$  is expressed as

$$\hat{n}_{m_a, \alpha}(\boldsymbol{\Omega}_m) = \hat{a}_{m_a, \alpha}^\dagger(\boldsymbol{\Omega}_m) \hat{a}_{m_a, \alpha}(\boldsymbol{\Omega}_m). \quad (19)$$

Using Eq. (17) the formula for density  $n_{ab}^{\alpha, \beta}$  of mean photon-pair numbers in Eq. (18) attains a simple form:

$$n_{ab}^{\alpha, \beta}(\boldsymbol{\Omega}_s, \boldsymbol{\Omega}_i) = |\phi_{ab}^{\alpha, \beta}(\boldsymbol{\Omega}_s, \boldsymbol{\Omega}_i)|^2. \quad (20)$$

A density  $n_{s, ab}^{\alpha, \beta}(\boldsymbol{\Omega}_s)$  of mean signal-photon numbers in the state  $|\psi\rangle_{s_a, i_b}^{\alpha, \beta}$  can easily be determined from the density  $n_{ab}^{\alpha, \beta}$  defined in Eq. (18) and using the relation in Eq. (20):

$$\begin{aligned}
n_{s, ab}^{\alpha, \beta}(\boldsymbol{\Omega}_s) &= \int_{-\pi/2}^{\pi/2} \sin(\vartheta_i) d\vartheta_i \int_{-\pi/2}^{\pi/2} d\psi_i \int_0^\infty d\omega_i \\
&|\phi_{ab}^{\alpha, \beta}(\boldsymbol{\Omega}_s, \boldsymbol{\Omega}_i)|^2. \quad (21)
\end{aligned}$$

If spectral resolution in detection of the signal-field transverse profile is not available, a spatial density  $n_{s, ab}^{\text{tr}, \alpha, \beta}(\vartheta_s, \psi_s)$  of mean signal-photon numbers emitted in the direction  $(\vartheta_s, \psi_s)$  is a useful characteristic. It can be derived using the density  $n_{s, ab}^{\alpha, \beta}$  of mean signal-photon numbers given in Eq. (21):

$$n_{s, ab}^{\text{tr}, \alpha, \beta}(\vartheta_s, \psi_s) = \int_0^\infty d\omega_s n_{s, ab}^{\alpha, \beta}(\boldsymbol{\Omega}_s). \quad (22)$$

The above densities can be analogously defined also for the idler field.

Spatial correlations between the signal- and idler-field photon numbers in their transverse planes can be quantified in terms of the fourth-order correlation functions  $n_{ab}^{\text{cor}, \alpha, \beta}(\vartheta_s, \psi_s, \vartheta_i, \psi_i)$  that give joint densities of photon-pair numbers such that a signal photon propagates along the  $(\vartheta_s, \psi_s)$  direction and the idler twin propagates along the  $(\vartheta_i, \psi_i)$  direction:

$$n_{ab}^{\text{cor}, \alpha, \beta}(\vartheta_s, \psi_s, \vartheta_i, \psi_i) = \int_0^\infty d\omega_s \int_0^\infty d\omega_i n_{ab}^{\alpha, \beta}(\boldsymbol{\Omega}_s, \boldsymbol{\Omega}_i). \quad (23)$$

Provided that the signal-photon propagation direction  $(\vartheta_s^0, \psi_s^0)$  is given, the joint density  $n_{ab}^{\text{cor}, \alpha, \beta}(\vartheta_s^0, \psi_s^0, \vartheta_i, \psi_i)$  remains a function of the idler-field emission angles  $\vartheta_i$  and  $\psi_i$  and its profile defines a correlated area. The correlated area of an idler photon determines an area in the idler-field transverse plane where an idler photon can be expected provided that its signal twin has been detected in the  $(\vartheta_s^0, \psi_s^0)$  direction.

Finally, an overall mean photon-pair number  $N_{ab}^{\alpha, \beta}$  related to the state  $|\psi\rangle_{s_a, i_b}^{\alpha, \beta}$  can be found using the following relation:

$$\begin{aligned}
N_{ab}^{\alpha, \beta} &= \prod_{m=s, i} \int_{-\pi/2}^{\pi/2} \sin(\vartheta_m) d\vartheta_m \int_{-\pi/2}^{\pi/2} d\psi_m \int_0^\infty d\omega_m \\
&n_{ab}^{\alpha, \beta}(\boldsymbol{\Omega}_s, \boldsymbol{\Omega}_i). \quad (24)
\end{aligned}$$

An important feature of layered structures is an increase of the efficiency of nonlinear process due to the enhanced electric-field amplitudes caused by interference along the  $z$  axis. This increase can be quantified with respect to a certain reference structure which fully exploits the nonlinearity, but does not rely on interference. In this reference structure, there occurs no back-scattering of the propagating fields and also the nonlinear process is assumed to be fully phase matched. The orientations of nonlinear layers and polarizations of the interacting fields are such that the most intense nonlinear effect occurs. This reference structure provides an ideal photon pair with a signal photon emitted in an arbitrary direction  $(\vartheta_s, \psi_s)$  and an idler photon in the corresponding  $(\vartheta_i, \psi_i)$  direction. Fixing  $\vartheta_s$  and  $\psi_s$ , the emitted pair can be described by the following output state  $|\psi\rangle_{s, i}^{\text{ref}}$  [compare Eq. (14)]:

$$\begin{aligned}
|\psi\rangle_{s, i}^{\text{ref}} &= -\frac{i}{2c^8} \int_0^\infty \omega_s^2 d\omega_s \int_0^\infty \omega_i^2 d\omega_i \sqrt{\omega_s \omega_i} \\
&\mathcal{E}_p(\omega_s + \omega_i) \sum_{l=1}^N \max(\mathbf{d}^{(l)}) L_l \hat{a}_s^\dagger(\omega_s) \hat{a}_i^\dagger(\omega_i) |\text{vac}\rangle, \quad (25)
\end{aligned}$$

where  $\hat{a}_s^\dagger(\omega_s)$  [ $\hat{a}_i^\dagger(\omega_i)$ ] stands for a signal- [idler-] field creation operator outside the reference structure. The function  $\max$  used in Eq. (25) gives the maximum value among the elements of tensor  $\mathbf{d}^{(l)}$ .

Using the reference structure a relative density  $\eta_{s, ab}^{\alpha, \beta}(\boldsymbol{\Omega}_s)$  of mean signal-photon numbers belonging to

the state  $|\psi\rangle_{s_a, i_b}^{\alpha, \beta}$  can naturally be defined as

$$\eta_{s, ab}^{\alpha, \beta}(\Omega_s) = \frac{n_{s, ab}^{\alpha, \beta}(\Omega_s)}{n_s^{\text{ref}}(\omega_s)}, \quad (26)$$

where the signal-field photon-number density  $n_{s, ab}^{\alpha, \beta}$  is written in Eq. (21). The reference signal-field photon-number density  $n_s^{\text{ref}}$  characterizes the state  $|\psi\rangle_{s, i}^{\text{ref}}$  in Eq. (25) and does not depend on the propagation angles  $\vartheta_s$  and  $\psi_s$ .

Properties of photon pairs in the time domain are complementary to those found in the spectral domain and belong to important characteristics of photon pairs. We can mention signal- and idler-field photon fluxes or coincidence-count interference patterns in different kinds of interferometers as examples. These photon-pair properties can be investigated, e.g., using the formulas contained in Sec. IIC of Ref. [37] even in this spatial vectorial model.

Numerical calculations that follow are performed for a cw pump field with a Gaussian transverse profile described as follows:

$$\begin{aligned} \mathcal{E}_p(\omega_p) &= \xi_p \delta(\omega_p - \omega_p^0), \\ \mathcal{E}_p^{\text{tr}}(k_x, k_y) &= \frac{r_p}{\sqrt{2\pi}} \exp\left[\frac{r_p^2(k_x^2 + k_y^2)}{4}\right]. \end{aligned} \quad (27)$$

In Eq. (27),  $\xi_p$  gives an amplitude of the pump field with the carrying frequency  $\omega_p^0$ ;  $r_p$  denotes the width of amplitude transverse profile. Normalization of the function  $\mathcal{E}_p^{\text{tr}}$  is such that  $\int dk_x \int dk_y |\mathcal{E}_p^{\text{tr}}(k_x, k_y)|^2 = 1$ . In case of cw pumping, there occur formulas in the above equations that contain a formal expression  $\delta^2(\omega)$ . This expression has to be replaced by the expression  $2T/(2\pi)\delta(\omega)$ , where the detection interval extends over  $(-T, T)$  and the limit  $T \rightarrow \infty$  may be considered.

### III. DESIGN OF AN EFFICIENT LAYERED STRUCTURE

Here we consider structures with odd numbers  $N$  of layers made of two kinds of materials. Layers of material  $b$  of length  $l_b$  are sandwiched by layers of material  $a$  having lengths  $l_a$ . Also pumping at a defined carrying frequency  $\omega_p^0$  and impinging on the structure at normal incidence is assumed. The down-converted signal and idler fields are assumed to have nearly degenerate frequencies.

We suggest a method for designing an efficient layered structure from the point of view of, in general, three-mode nonlinear interaction. It is based on two observations:

- An efficient nonlinear process occurs provided that all three nonlinearly interacting fields lie inside their transmission peaks. This behavior originates in the fact that the electric-field amplitudes of

monochromatic fields with frequencies in transmission peaks are enhanced inside the structure owing to constructive interference of back-scattered light. It follows from the band-gap theory that the closer the transmission peak to a band gap, the greater the electric-field amplitudes.

- As numerical calculations have revealed, the overlap integral over the amplitudes of three interacting fields giving the strength of the effective nonlinear interaction [see Eq. (1)] vanishes if the signal- and idler-field amplitudes along the structure are the same. This means that photon-pair states degenerate in frequencies, emitted in symmetric directions and having the same polarizations cannot be generated.

We note that these facts have been found crucial in designing layered structures efficient for second-harmonic generation [50]. Considering a collinear interaction, the requirements are even more strict because of only one propagation direction. This requires specific approaches that rely, e.g., on tuning the frequencies of transmission peaks by changing the index of refraction of one type of the layers [50]. Alternatively, non-collinear second-harmonic generation has been considered. In this case, there exists one free parameter (radial emission angle) that can be varied in order to find an efficient structure. This represents an equivalent problem to that considered here and can be treated by the developed systematic approach.

Returning back to the considered layered structures they are characterized by three parameters: number  $N$  of layers and lengths  $l_a$  and  $l_b$  of these layers. A detailed inspection has revealed that the number  $N$  of layers significantly determines the number of generated photon pairs as well as angular extensions of the emission areas of photons in a pair (see Fig. 3 below). The greater the number  $N$  of layers the greater the number of generated photon pairs and also the smaller the angular extensions of emission areas. From practical point of view, the number  $N$  of layers is approximately fixed considering these dependencies. Having the number  $N$  of layers fixed, there remain two adjustable parameters - layers' lengths  $l_a$  and  $l_b$ . However, these two lengths cannot be chosen arbitrarily because the pump field at the carrying frequency  $\omega_p^0$  has to be in a transmission peak.

Let us fix the lengths  $l_a$  and  $l_b$  (together with the number  $N$  of layers) for a moment and determine the spectral intensity transmission  $T(\omega)$  along the  $+z$  direction (of the pump-field propagation) using, e.g., the transfer-matrix formalism [43]. Increasing the frequency  $\omega$  there occur forbidden bands one following the other. The difference in central frequencies of the neighbor forbidden bands is roughly the same in accord with the band-gap theory. This may be convenient for spectrally nearly degenerate SPDC provided that the process of SPDC can be tuned such that the pump-field frequency lies inside a transmission peak close to the second forbidden band

whereas the signal- and idler-field frequencies are inside the transmission peaks near to the first forbidden band. We note that all three interacting fields can accommodate themselves either to the transmission peaks above or below the forbidden bands. This helps to obey the quite strong requirements of the three-field interaction by varying the signal-field emission angle  $\vartheta_s$ . However, suitable conditions can only be revealed numerically.

Now we return back to the problem in which the pump-field carrying frequency  $\omega_p^0$  is fixed. As follows from the considerations of the previous paragraph, useful structures are those that have the first upper or the first lower transmission peak near to the second forbidden band at the pump-field carrying frequency  $\omega_p^0$ . Inspection of the behavior of structures with different layers' lengths  $l_a$  and  $l_b$  has shown that there exists a system of curves in the plane spanned by layers' lengths  $l_a$  and  $l_b$  that provides the required transmission peaks at the frequency  $\omega_p^0$ . One curve corresponds to the first lower transmission peak of the second forbidden band. Similarly, another curve is associated with the first upper transmission peak of the second forbidden band. They can be revealed as follows using the scaling property of diffraction phenomena in optics.

We consider a fictitious dispersion-free structure with the indexes of refraction appropriate for the pump-field frequency  $\omega_p^0$  and define the corresponding optical lengths  $l_a^{\text{opt}}$  and  $l_b^{\text{opt}}$ . It can be shown that the ratio  $L = l_b^{\text{opt}}/l_a^{\text{opt}}$  of optical lengths represents a suitable variable for parametrization of these curves. Suitable optical lengths  $l_a^{\text{opt}}$  and  $l_b^{\text{opt}}$  for a given value of the ratio  $L$  can be revealed easily using the scaling property of diffraction phenomena. We fix the value of length  $l_a^{\text{opt}}$  to, e.g.,  $l_a^{\text{opt},0} = \lambda_p^0/2 = \pi c/\omega_p^0$ . This gives the unit length of diffraction phenomena that can be, in principle, chosen arbitrarily. As the ratio  $L$  is given, the optical length  $l_b^{\text{opt},0}$  is derived as  $l_b^{\text{opt},0} = Ll_a^{\text{opt},0}$  and we can calculate the spectral intensity transmission  $T_p(\omega_p)$  for this structure. We further identify the frequency  $\omega_p^{\text{max}}$  of the first lower (or upper) transmission peak of the second forbidden band. Then we have to 'transfer' the actual frequency  $\omega_p^{\text{max}}$  of the transmission peak to the required frequency  $\omega_p^0$  using the scaling property. The scaling property provides the layers' optical lengths in the form:  $l_a^{\text{opt}} = l_a^{\text{opt},0}\omega_p^0/\omega_p^{\text{max}}$  and  $l_b^{\text{opt}} = Ll_a^{\text{opt}}$ . We note that the obtained lengths differ for the lower and the upper transmission peaks.

In the next step we move along the obtained two curves (for the upper and the lower transmission peaks) parameterized by the ratio  $L$  and numerically analyze the structures. The maximum  $\eta_s^{\text{max}}$  of relative density  $\eta_s(\omega_s, \vartheta_s, \psi_s^0)$  of mean signal-photon numbers taken over the signal-field frequency  $\omega_s$  and radial emission angle  $\vartheta_s$  assuming the fixed signal-field azimuthal emission angle  $\psi_s^0$  has been found a suitable quantity for monitoring efficiency of the nonlinear process. The signal- and idler-field polarizations are assumed to be fixed. The greater the value of maximum  $\eta_s^{\text{max}}$  of relative density the closer

the signal- and idler-field transmission peaks to the first forbidden band. A curve giving the dependence of maximum  $\eta_s^{\text{max}}$  of relative density on the ratio  $L$  is thus a good indicator for choosing suitable layers' lengths. We note that the curve depends on polarization properties of the signal and idler fields as well as the azimuthal signal-field emission angle  $\psi_s^0$ . It is also possible to monitor another quantity in this procedure, e.g., the overall mean photon-pair number  $N$  given in Eq. (24). Or the density of mean signal-photon numbers emitted for a fixed azimuthal emission angle  $\psi_s^0$  and determined as  $\int_{-\pi/2}^{\pi/2} \sin(\vartheta_s) d\vartheta_s n_s^{\text{tr}}(\vartheta_s, \psi_s)$  using the formula in Eq. (22) may be considered.

As an example, the dependence of maximum  $\eta_s^{\perp, \parallel, \text{max}}$  of relative density of two photons propagating along the  $+z$  axis on the ratio  $L$  for the first lower and the first upper pump-field transmission peak of the second forbidden band of the structure composed of 11 and 101 layers, respectively, is plotted in Fig. 2 (for details, see below). The curve in Fig. 2(a) appropriate for the structure with 11 layers is continuous and rather flat. This means that there exists a whole continuous set of structures giving an efficient nonlinear process. On the other hand, efficient nonlinear structures with  $N = 101$  layers are found only in peaks of the curve in Fig. 2(b). This is a consequence of complex interference of back-scattered light inside these structures. We note that the appropriate transmission peaks in all three interacting fields do not necessarily exist for all values of the ratio  $L$ . Also the greatest values of maximum  $\eta_s^{\perp, \parallel, \text{max}}$  of the relative density are found for the values of ratio  $L$  in a certain restricted region. As the graph in Fig. 2(b) shows, the greatest values of maximum  $\eta_s^{\perp, \parallel, \text{max}}$  occur around  $L = 0.5$ .

The curves in Fig. 2 demonstrate a 'weak' increase of values of the maximum  $\eta_s^{\perp, \parallel, \text{max}}$  of relative signal-field density with the increasing values of the number  $N$  of layers. As the densities  $n_s^{\text{ref}}$  of the mean signal-photon numbers of the reference structure are linearly proportional to the second power of the length of nonlinear material inside the structure, the densities  $n_s$  of the mean signal-photon numbers increase better than  $N^2$ . This is very important, because the mean number of emitted photon pairs increases less than the second power of the length of nonlinear material in other structures producing photon pairs like bulk crystals, periodically-poled crystals or wave-guiding structures because of 'longitudinal' phase-matching conditions. Nearly linear dependence of the mean photon-pair numbers on the length of a nonlinear structure is commonly observed.

#### IV. INTENSITY TRANSVERSE PROFILES AND CORRELATED AREAS

We consider three examples of layered structures made of GaN/AlN that demonstrate typical features of the emitted photon pairs. They generate photon pairs with



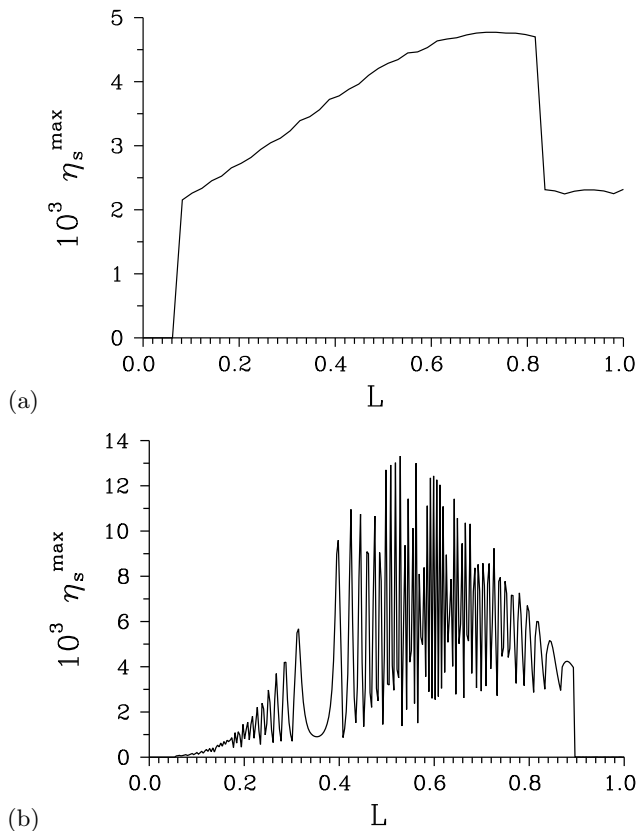


FIG. 2: Maximum  $\eta_s^{\perp, \parallel, \max}$  of the relative density of mean signal-photon numbers for states with photons propagating forward as a function of the ratio  $L$  of optical layers' lengths for the first lower [upper] pump-field transmission peak of the second forbidden band for the structure with  $N = 11$  [ $N = 101$ ] layers;  $\psi_s^0 = 0$  deg.

different polarizations of the signal and idler photons. They are designed in such a way that three different mechanisms of splitting the correlated area are observed. The pump field propagating at normal incidence at the carrying wavelength  $\lambda_p^0 = 400$  nm is assumed. The signal and idler fields are emitted around the degenerate wavelengths  $\lambda_s^0 = \lambda_i^0 = 800$  nm in non-collinear geometry. The GaN and AlN layers are positioned such that their optical axes are perpendicular to the boundaries. The considered structures differ in the number  $N$  of layers ( $N = 11, 51$  and  $101$ ). This results in different signal-field intensity transverse profiles plotted in Fig. 3. Whereas the shortest structure with  $N = 11$  layers has only one emission area, the longest one with  $N = 101$  layers already forms five emission rings. We note that transverse profiles of the down-converted fields can also be efficiently tailored by modifying the pump-beam profile [14].

The analyzed structures have certain properties in common. Namely, they cannot generate proton pairs in nearly collinear geometries because of the symmetry that cancels the overlap integral. As for correlated areas, their azimuthal spreads  $\Delta\psi_i$  depend on the width  $r_p$  of transverse pump-field profile [18, 51]. The radial spreads  $\Delta\vartheta_i$

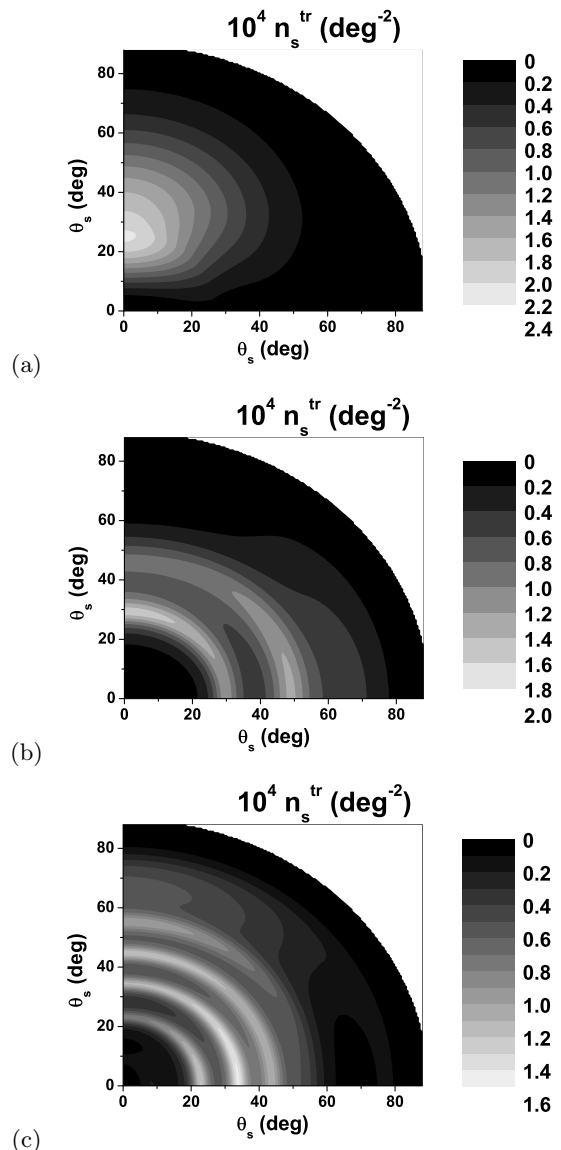


FIG. 3: Densities  $n_s^{\text{tr}}$  of mean signal-photon numbers depending on signal-field radial ( $\vartheta_s$ ) and azimuthal ( $\psi_s$ ) emission angles for (a)  $N = 11$ , (b)  $N = 51$  and (c)  $N = 101$  layers without polarization resolution for both photons propagating forward. The emitted signal field is projected onto a hemisphere, one quadrant of which is plotted. In the graphs, the radial emission angle  $\vartheta_s$  determines the distance from the origin, whereas the azimuthal emission angle  $\psi_s$  gives the rotation measured from the vertical direction. Behavior of the density  $n_s^{\text{tr}}$  in the remaining three quadrants can be derived from symmetry. The density  $n_s^{\text{tr}}$  is normalized such that  $\int_0^{\pi/2} \sin(\vartheta_s) d\vartheta_s \int_{-\pi/2}^0 d\psi_s n_s^{\text{tr}}(\vartheta_s, \psi_s) = (\pi/180)^2/4$ ;  $r_p \rightarrow \infty$ .

depend also on the geometry of the layered structure; the greater the number  $N$  of layers, the smaller the correlated area. In more detail, the considered structures behave as follows.

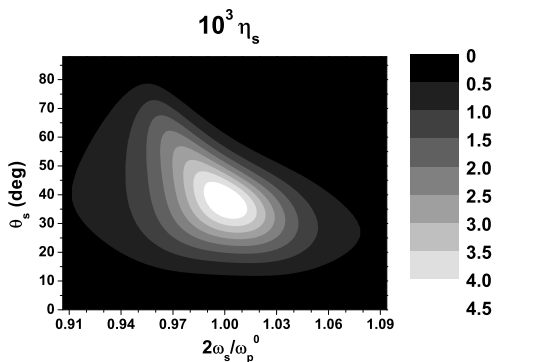


FIG. 4: Relative density  $\eta_s$  of mean signal-photon numbers depending on normalized signal-field frequency  $2\omega_s/\omega_p^0$  and radial emission angle  $\vartheta_s$  for the structure with  $N = 11$  layers for both photons with arbitrary polarizations propagating forward;  $\psi_s = 0$  deg,  $r_p \rightarrow \infty$ .

### A. Structure with 11 layers

The structure is composed of 6 nonlinear GaN layers 90.14 nm long and 5 linear AlN layers 74.92 nm long. Despite a relatively small number of layers, photonic band gaps are already formed though the bottoms of forbidden bands have intensity transmissions around 0.3. For  $\psi_s = 0$  deg, an efficient SPDC occurs for polarizations (TE,TM,TE) and (TE,TE,TM) for the (pump,signal,idler) fields due to the nonlinear coefficient  $d(1,1,3)$ . The fields are tuned to the first lower transmission peaks of the first and second forbidden bands, so the efficiency of SPDC is nearly optimal. The signal and idler transmission peaks are spectrally broad and, as a consequence, we observe one large emission area in the signal-field transverse plane that extends from cca  $\vartheta_s = 20$  deg to 60 deg [see Fig. 3(a)]. The relative density  $\eta_s$  of mean signal-photon numbers as plotted in Fig. 4 reveals that the emitted photons have nearly degenerate frequencies and relatively broad spectra. The shape of relative density  $\eta_s$  as shown in Fig. 4 is caused by a different radial dependence of intensity transmissions  $T_{TE}$  and  $T_{TM}$ . In the area around  $\psi_s = \pm 90$  deg there occurs no photon-pair generation because of geometric reasons (the propagation of signal and idler fields as TM waves is not supported). Compared to one GaN layer  $6 \times 90.14$  nm long, the structure gives cca 2 times greater relative densities  $\eta_s$ .

The correlated area of an idler photon for a collimated pump beam is composed of several 'islands' localized around different idler-field radial emission angles  $\vartheta_i$  [see Fig. 5(a)]. This breaking is caused by the zig-zag movement of two photons inside the structure after being generated in one layer. The comparison of correlated areas for collimated and focused pump beams using, e.g., the graphs in Fig. 5(a) and (b) reveals that the spread of correlated area along the azimuthal emission angle  $\psi_i$  depends strongly on the amount of focusing the pump

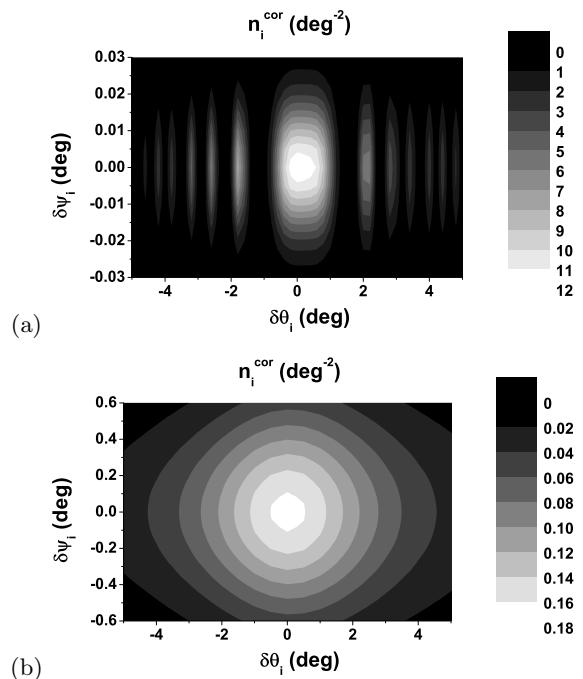


FIG. 5: Correlated area  $n_i^{\text{cor}}(\vartheta_i, \psi_i)$  of an idler photon for (a)  $r_p = 1$  mm and (b)  $r_p = 30$  nm belonging to a signal photon propagating along direction  $\vartheta_s^0 = 38$  deg and  $\psi_s^0 = 0$  deg. Both photons with arbitrary polarizations propagate forward;  $\vartheta_i = \vartheta_i^0 + \delta\vartheta_i$ ,  $\vartheta_i^0 = -\vartheta_s^0$ ,  $\psi_i = \psi_i^0 + \delta\psi_i$ ,  $\psi_i^0 = -\psi_s^0$ . The normalization  $\int_{-\pi/2}^{\pi/2} d\vartheta_i \int_{-\pi/2}^{\pi/2} d\psi_i n_i^{\text{cor}}(\vartheta_i, \psi_i) = (\pi/180)^2$  is used.

beam. On the other hand, the shape of correlated area in the radial emission angle  $\vartheta_i$  is blurred by a focused pump beam keeping the overall spread of correlated area roughly the same.

### B. Structure with 51 layers

The second structure contains 26 nonlinear GaN layers 106.87 nm long and 25 linear AlN layers 65.99 nm long. This structure has already well-formed forbidden bands. As Fig. 3(b) shows there occurs an efficient SPDC in two concentric rings in the transverse plane. The structure is designed such that an efficient nonlinear interaction for fields' polarizations (TM,TM,TM) occurs along the direction  $\psi_s = 0$  deg using the nonlinear coefficient  $d(2,2,3)$ . The pump field lies in the first upper transmission peak of the second forbidden band and the signal and idler fields are in the first and second lower transmission peaks of the first forbidden band. The relative density  $\eta_s$  of mean signal-photon numbers as plotted in Fig. 6 demonstrates that the signal-field (and also idler-field) intensity spectra are composed of two symmetric peaks. There occurs no photon-pair generation for degenerate signal- and idler-field frequencies because of symmetry. This indicates the generation of photon pairs in the state that is anti-symmetric with respect to the exchange of the

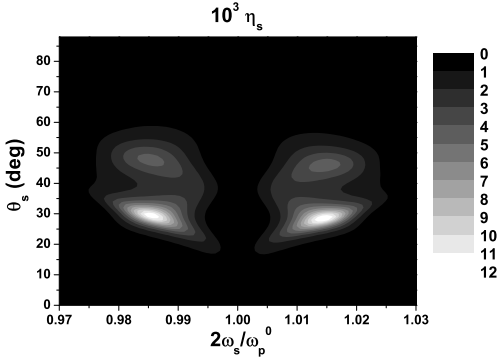


FIG. 6: Relative density  $\eta_s$  of mean signal-photon numbers as it depends on normalized signal-field frequency  $2\omega_s/\omega_p^0$  and radial emission angle  $\vartheta_s$  analyzing the structure with  $N = 51$  layers and both forward-propagating photons with arbitrary polarizations;  $\psi_s = 0$  deg,  $r_p \rightarrow \infty$ .

signal- and idler-field frequencies. Anti-bunching of photons in a pair and anti-coalescence (observed in a Hong-Ou-Mandel interferometer) are the distinguished features of this state [46]. The graph in Fig. 3(b) reveals that an efficient SPDC occurs also for azimuthal emission angles  $\psi_s$  around  $\pm 90$  deg. In this case, the signal photon is generated as TE wave and the idler photon as TM wave or vice versa. The structure gives cca 50 times greater relative densities  $\eta_s$  in comparison with one GaN layer  $26 \times 106.87$  nm long.

As a consequence of two-peak structure of the signal- and idler-field spectra there occurs splitting of the correlated area of an idler photon, as documented in Fig. 7(a). The overall correlated area is composed of two symmetric parts. Because this splitting arises from symmetry, it survives even for focused pump beams, as demonstrated in Fig. 7(b).

### C. Structure with 101 layers

The last structure is composed of 51 nonlinear GaN layers 106.42 nm long and 50 linear AlN layers 65.71 nm long. The pump field lies in the first upper transmission peak of the second forbidden band. A detailed comparison of the relative density  $\eta_s$  of mean signal-photon numbers (see Fig. 8) with intensity transmission spectra  $T_{TE}$  and  $T_{TM}$  valid for TE and TM waves, respectively, and obtained for  $\psi = 0$  deg (see Fig. 9) reveals the following. An efficient SPDC occurs at intersections of  $j$ th and  $(j+1)$ th lower transmissions peaks of the first forbidden band for  $j = 2, 3, 4, 5, 6$ . This results in five concentric rings in the density  $n_s^{tr}$  of mean signal-photon numbers clearly visible in Fig. 3(c). We note that the nonlinear coefficient  $d(1, 1, 3)$  is exploited here and (TE, TM, TE) and (TE, TE, TM) [(TM, TM, TM)] polarizations are suitable for the angles around  $\psi_s = 0$  deg [ $\psi_s = \pm 90$  deg]. The relative density  $\eta_s$  of mean signal-photon numbers indicates that the signal-field intensity spectra are com-

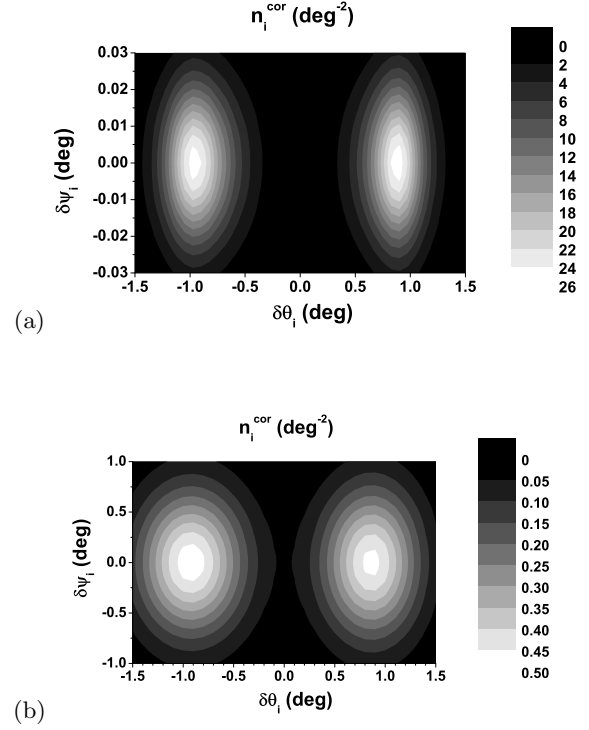


FIG. 7: Correlated area  $n_i^{cor}(\vartheta_i, \psi_i)$  of an idler photon for (a)  $r_p = 1$  mm and (b)  $r_p = 30$  nm corresponding to a signal photon propagating along direction  $\vartheta_s^0 = 29$  deg and  $\psi_s^0 = 0$  deg;  $N = 51$ . Both photons of arbitrary polarizations propagate forward;  $\vartheta_i = \vartheta_i^0 + \delta\vartheta_i$ ,  $\vartheta_i^0 = -\vartheta_s^0$ ,  $\psi_i = \psi_i^0 + \delta\psi_i$ ,  $\psi_i^0 = -\psi_s^0$ .

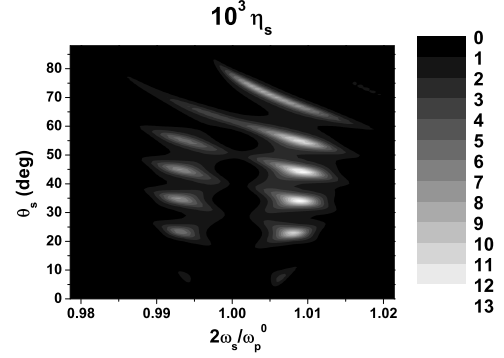


FIG. 8: Relative density  $\eta_s$  of mean signal-photon numbers depending on normalized signal-field frequency  $2\omega_s/\omega_p^0$  and radial emission angle  $\vartheta_s$ . The structure with  $N = 101$  layers and both photons of arbitrary polarizations propagating forward are assumed;  $\psi_s = 0$  deg,  $r_p \rightarrow \infty$ .

posed of two peaks of different weights for  $\psi_s = 0$  deg. One peak is related to a TE signal-field wave, whereas the second one arises from a TM signal-field wave. Comparison with one GaN layer  $51 \times 106.42$  nm long reveals that the enhancement of optical fields inside the structure results in an increase of the relative density  $\eta_s$  cca 330 times.

A two-peak spectral structure leads to splitting of the

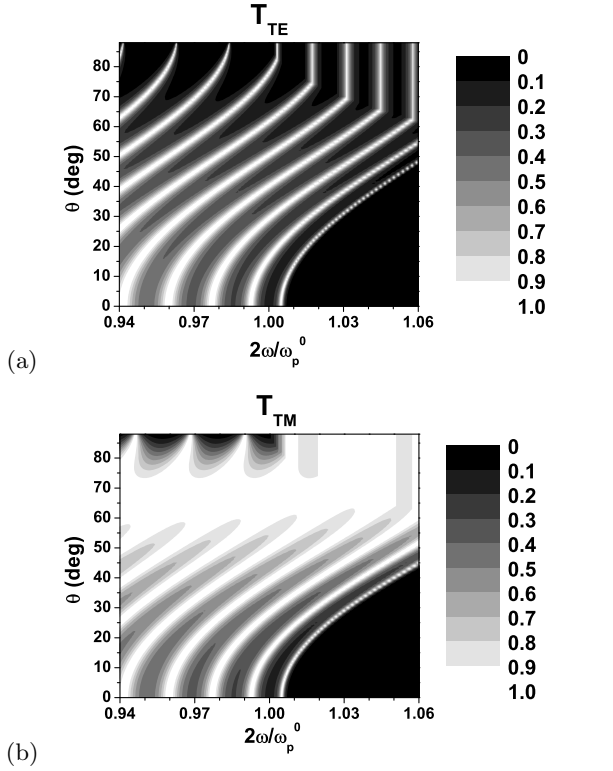


FIG. 9: Intensity transmission coefficients  $T_{TE}$  for TE waves [(a)] and  $T_{TM}$  for TM waves [(b)] as they depend on radial emission angle  $\vartheta$  assuming  $\psi = 0$  deg and the structure with  $N = 101$  layers. For  $\psi = \pm 90$  deg, the graphs for TE and TM polarizations are mutually exchanged.

correlated area of the idler photon into two parts [52], as shown in Fig. 10(a). However, two parts are not symmetric in this case and they can also merge together provided that the pump beam is sufficiently focused [see Fig. 10(b)]. The distance between two parts in the idler-photon radial emission angle  $\vartheta_i$  increases with the increasing signal-photon radial emission angle  $\vartheta_s^0$ . Whereas this distance equals cca 0.6 deg for  $\vartheta_s^0 = 23$  deg (the first ring), it equals already cca 4 deg for  $\vartheta_s^0 = 66$  deg (the fifth ring). Idler photons found in different parts of the correlated area differ in their polarizations.

The above investigated structures demonstrate main features of photon pairs generated in nonlinear layered structures. These structures allow to generate photon pairs entangled in frequencies, polarizations as well as in emission directions. Moreover, they allow tailoring of properties of photon pairs varying namely the number of layers. A small amount of nonlinear material inside them is compensated by an increase of electric-field amplitudes originating in fields' back-scattering.

## V. CONCLUSIONS

We have developed a spatial vectorial quantum model of spontaneous parametric down-conversion in nonlin-

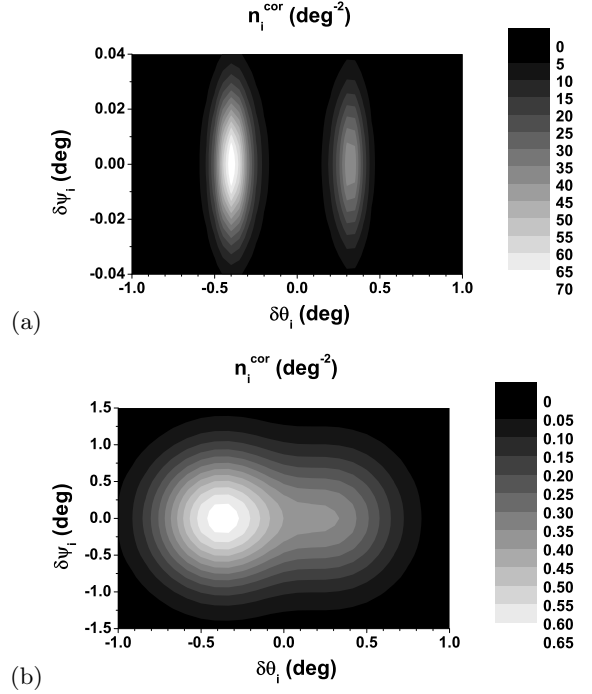


FIG. 10: Correlated area  $n_i^{cor}(\vartheta_i, \psi_i)$  of an idler photon for (a)  $r_p = 1$  mm and (b)  $r_p = 30$  nm belonging to a signal photon propagating along direction  $\vartheta_s^0 = 23$  deg and  $\psi_s^0 = 0$  deg. Both photons have arbitrary polarizations and propagate forward;  $\vartheta_i = \vartheta_i^0 + \delta\vartheta_i$ ,  $\vartheta_i^0 = -\vartheta_s^0$ ,  $\psi_i = \psi_i^0 + \delta\psi_i$ ,  $\psi_i^0 = -\psi_s^0$ .

ear layered structures. Photon pairs generated in these structures can be entangled in frequencies, polarizations as well as emission directions. Namely entanglement in emission directions is important because it can be efficiently tailored varying the number of layers. A method for designing efficient layered structures has been suggested. Its efficiency has been demonstrated suggesting three typical structures. It has been shown that the number of generated photon-pairs increases greater than the second power of the number of layers. Signal-field intensity profiles and correlated areas in the transverse plane have been analyzed in the designed structures. Intensity profiles are typically composed of concentric rings. The greater the number of layers, the greater the number of rings. Correlated areas may be broken into several parts because of three possible reasons: i) Zig-zag movement of photons inside the structure, ii) Necessity to obey geometric symmetries, and iii) Polarization-dependent properties. Splitting of the correlated area arising from the geometric symmetry survives even for a focused pump beam. Also states of photon pairs showing anti-bunching and anti-coalescence can efficiently be generated in layered structures. We believe that nonlinear layered structures are potentially interesting namely as efficient sources of photon-pair fields entangled in propagation directions which might be useful, e.g., in 'parallel processing' of quantum information.

### Acknowledgments

Support by projects IAA100100713 of GA AV ĀR and COST OC 09026, 1M06002 and Operational Program

Research and Development for Innovations - European Social Fund (project CZ.1.05/2.1.00/03.0058) of the Ministry of Education of the Czech Republic is acknowledged. The author thanks M. Centini for useful discussions.

- 
- [1] C. K. Hong, Z. Y. Ou, and L. Mandel, *Phys. Rev. Lett.* **59**, 2044 (1987).
- [2] L. Mandel and E. Wolf, *Optical Coherence and Quantum Optics* (Cambridge Univ. Press, Cambridge, 1995).
- [3] in *The Physics of Quantum Information*, edited by D. Bouwmeester, A. Ekert, and A. Zeilinger (Springer, Berlin, 2000).
- [4] J. Peřina, Z. Hradil, and B. Jurčo, *Quantum Optics and Fundamentals of Physics* (Kluwer, Dordrecht, 1994).
- [5] D. Bouwmeester, J. W. Pan, K. Mattle, M. Eibl, H. Weinfurter, and A. Zeilinger, *Nature* **390**, 575 (1997).
- [6] S. E. Harris, *Phys. Rev. Lett.* **98**, 063602 (2007).
- [7] G. Brida, M. V. Chekhova, I. P. Degiovanni, M. Genovese, G. K. Kitaeva, A. Meda, and O. A. Shumilkina, *Phys. Rev. Lett.* **103**, 193602 (2009).
- [8] T. E. Keller and M. H. Rubin, *Phys. Rev. A* **56**, 1534 (1997).
- [9] J. Peřina Jr., A. V. Sergienko, B. M. Jost, B. E. A. Saleh, and M. C. Teich, *Phys. Rev. A* **59**, 2359 (1999).
- [10] A. Joobeur, B. E. A. Saleh, and M. C. Teich, *Physical Review A* **50**, 3349 (1994).
- [11] A. Joobeur, B. E. A. Saleh, T. S. Larchuk, and M. C. Teich, *Physical Review A* **53**, 4360 (1996).
- [12] G. Vallone, E. Pomarico, P. Mataloni, F. De Martini, and V. Berardi, *Phys. Rev. Lett.* **98**, 180502 (2007).
- [13] C. H. Monken, P. H. Souto Ribeiro, and S. Padua, *Phys. Rev. A* **57**, 3123 (1998).
- [14] S. P. Walborn, A. N. de Oliveira, R. S. Thebaldi, and C. H. Monken, *Phys. Rev. A* **69**, 023811 (2004).
- [15] C. K. Law and J. H. Eberly, *Phys. Rev. Lett.* **92**, 127903 (2004).
- [16] A. Mair, A. Vaziri, G. Weihs, and A. Zeilinger, *Nature* **412**, 313 (2001).
- [17] S. S. R. Oemrawsingh, X. Ma, D. Voigt, A. Aiello, E. R. Eliel, G. W. t Hooft, and J. P. Woerdman, *Phys. Rev. Lett.* **95**, 240501 (2005).
- [18] G. Molina-Terriza, S. Minardi, Y. Deyanova, C. I. Osorio, M. Hendrych, and J. P. Torres, *Phys. Rev. A* **72**, 065802 (2005).
- [19] B. M. Jost, A. V. Sergienko, A. F. Abouraddy, B. E. A. Saleh, and M. C. Teich, *Opt. Express* **3**, 81 (1998).
- [20] O. Haderka, J. Peřina Jr., and M. Hamar, *J. Opt. B: Quantum Semiclass. Opt.* **7**, S572 (2005).
- [21] M. H. Rubin and Y. H. Shih, *Phys. Rev. A* **78**, 033836 (2008).
- [22] E. Brambilla, A. Gatti, M. Bache, and L. A. Lugiato, *Phys. Rev. A* **69**, 023802 (2004).
- [23] O. Jedrkiewicz, Y. K. Jiang, E. Brambilla, A. Gatti, M. Bache, L. A. Lugiato, and P. Di Trapani, *Phys. Rev. Lett.* **93**, 243601 (2004).
- [24] A. Migdall, *Physics Today* **41**, 1 (1999).
- [25] D. Bruß and N. Lütkenhaus, in *Applicable Algebra in Engineering, Communication and Computing, Vol. 10* (Springer, Berlin, 2000), p. 383.
- [26] G. K. Kitaeva, *Phys. Rev. A* **76**, 043841 (2007).
- [27] J. Svozilík and J. Peřina Jr., *Phys. Rev. A* **80**, 023819 (2009).
- [28] J. Svozilík and J. Peřina Jr., *Opt. Express* **18**, 27130 (2010).
- [29] A. B. URen, C. Silberhorn, K. Banaszek, and I. A. Walmsley, *Phys. Rev. Lett.* **93**, 093601 (2004).
- [30] S. M. Spillane, M. Fiorentino, and R. G. Beausoleil, *Opt. Express* **15**, 8770 (2007).
- [31] J. Chen, A. J. Pearlman, A. Ling, J. Fan, and A. Migdall, *Opt. Express* **17**, 6727 (2009).
- [32] in *Nanoscale Linear and Nonlinear Optics, AIP Vol. 560*, edited by M. Bertolotti, C. M. Bowden, and C. Sibilias (AIP, Melville, 2001).
- [33] E. Yablonovitch, *Phys. Rev. Lett.* **58**, 2059 (1987).
- [34] S. John, *Phys. Rev. Lett.* **58**, 2486 (1987).
- [35] A. N. Vamivakas, B. E. A. Saleh, A. V. Sergienko, and M. C. Teich, *Phys. Rev. A* **70**, 043810 (2004).
- [36] M. Centini, J. Peřina Jr., L. Sciscione, C. Sibilias, M. Scalora, M. J. Bloemer, and M. Bertolotti, *Phys. Rev. A* **72**, 033806 (2005).
- [37] J. Peřina Jr., M. Centini, C. Sibilias, M. Bertolotti, and M. Scalora, *Phys. Rev. A* **73**, 033823 (2006).
- [38] X. Li, P. L. Voss, J. E. Sharping, and P. Kumar, *Phys. Rev. Lett.* **94**, 053601 (2005).
- [39] J. Fulconis, O. Alibart, W. Wadsworth, P. Russell, and J. Rarity, *Opt. Express* **13**, 7572 (2005).
- [40] J. Fan, A. Migdall, and L. J. Wang, *Opt. Lett.* **30**, 3368 (2005).
- [41] P. Abolghasem, M. Hendrych, X. Shi, J. P. Torres, and A. S. Helmy, *Opt. Lett.* **34**, 2000 (2009).
- [42] J. Svozilík, M. Hendrych, A. S. Helmy, and J. P. Torres, *Opt. Express* **19**, 3115 (2011).
- [43] P. Yeh, *Optical Waves in Layered Media* (Wiley, New York, 1988).
- [44] J. Peřina Jr., M. Centini, C. Sibilias, and M. Bertolotti, *J. Russ. Laser Res.* **30**, 508 (2009).
- [45] J. Peřina Jr., M. Centini, C. Sibilias, and M. Bertolotti, *Phys. Rev. A* **80**, 033844 (2009).
- [46] J. Peřina Jr., M. Centini, C. Sibilias, M. Bertolotti, and M. Scalora, *Phys. Rev. A* **75**, 013805 (2007).
- [47] W. Vogel, D. G. Welsch, and S. Walentowicz, *Quantum Optics* (Wiley-VCH, Weinheim, 2001).
- [48] J. Peřina Jr., A. Lukš, O. Haderka, and M. Scalora, *Phys. Rev. Lett.* **103**, 063902 (2009).
- [49] J. Peřina Jr., A. Lukš, and O. Haderka, *Phys. Rev. A* **80**, 043837 (2009).
- [50] M. Scalora, M. J. Bloemer, A. S. Manka, J. P. Dowling, C. M. Bowden, R. Viswanathan, and J. W. Haus, *Phys. Rev. A* **56**, 3166 (1997).
- [51] M. Hamar, J. Peřina Jr., O. Haderka, and V. Michálek, *Phys. Rev. A* **81**, 043827 (2010).
- [52] J. Peřina Jr., M. Centini, C. Sibilias, M. Bertolotti, and M. Scalora, in *Conference on Coherence and Quantum Optics* (Optical Society of America, 2007), p. CSuA6.